

A SUPER-EARTH TRANSITING A NAKED-EYE STAR*

JOSHUA N. WINN¹, JAYMIE M. MATTHEWS², REBEKAH I. DAWSON³, DANIEL FABRYCKY^{4,5}, MATTHEW J. HOLMAN³,
 THOMAS KALLINGER^{2,6}, RAINER KUSCHNIG⁶, DIMITAR SASSELOV³, DIANA DRAGOMIR⁵, DAVID B. GUENTHER⁷,
 ANTHONY F. J. MOFFAT⁸, JASON F. ROWE⁹, SLAVEK RUCINSKI¹⁰, WERNER W. WEISS⁶

Submitted to ApJ Letters

ABSTRACT

We have detected transits of the innermost planet “e” orbiting 55 Cnc ($V = 6.0$), based on two weeks of precise photometric monitoring with the *MOST* space telescope. The transits of 55 Cnc e occur with the period (0.74 d) and phase that had been predicted by Dawson & Fabrycky, and with the expected duration and depth for the crossing of a Sun-like star by a hot super-Earth. Assuming the star’s mass and radius to be $0.96 \pm 0.10 M_{\odot}$ and $1.10 \pm 0.10 R_{\odot}$, the planet’s mass, radius, and mean density are $8.57 \pm 0.64 M_{\oplus}$, $1.63 \pm 0.16 R_{\oplus}$, and $10.9 \pm 3.1 \text{ g cm}^{-3}$. The high density suggests the planet has a rock-iron composition as opposed to hydrogen, water, or other light elements. This makes 55 Cnc e similar to the other transiting super-Earths in tight orbits around G stars (Kepler-10b and Corot-7b), and unlike the lower-density super-Earths that are less strongly irradiated (GJ 1214b and Kepler-11d,e,f). The host star of 55 Cnc e is far brighter than that of any other known transiting planet, which will facilitate further investigations.

Subject headings: planetary systems — planets and satellites: formation, interiors — stars: individual (55 Cnc)

1. INTRODUCTION

Precise Doppler observations have revealed five planets orbiting the nearby G8 V star 55 Cnc (Butler et al. 1997, Marcy et al. 2002, McArthur et al. 2004, Wisdom 2005, Fischer et al. 2008). Only a few other stars are known to host as many planets: HD 10180 (Lovis et al. 2011), Kepler-11 (Lissauer et al. 2011), and the Sun. Among the other reasons why 55 Cnc has attracted attention are the 3:1 resonance between two of its planets (Ji et al. 2003), the existence of an M dwarf companion at a distance of 10^3 AU (Mugrauer et al. 2006), and the unusually low mass and short period of its innermost planet, designated “e”.

McArthur et al. (2004) reported a period and minimum mass for 55 Cnc e of 2.808 d and $14.2 M_{\oplus}$, respectively. Those parameters were confirmed by Fischer et al. (2008). More recently, Dawson & Fabrycky (2010) argued that 55 Cnc e had been mischaracterized due to aliasing in the radial-velocity data, and that the true period and minimum mass are 0.74 d and $8.3 M_{\oplus}$.

One implication of the shorter period would be an increased

transit probability, from 13% to 33%. The occurrence of transits enhances the importance of an exoplanetary system, because photometric and spectroscopic observations of transits can reveal a wealth of details about the planet’s dimensions, atmosphere, and orbit (see, e.g., Winn 2010).

Fischer et al. (2008) searched for transits in their 11-year photometric record, ruling out transits for planets b ($P = 14.7$ d) and c (44.3 d). However, the time coverage was not complete enough to rule out transits for planets f (260 d) and d (5200 d), and the precision was insufficient to detect transits of the smallest planet e.

Here we present space-based photometry of 55 Cnc revealing a transit signal with the characteristics predicted by Dawson & Fabrycky (2010). Section 2 presents the data, and Section 3 presents the light curve analysis, yielding estimates for the mass, radius, and density of the planet. In Section 4 we place 55 Cnc e in the context of the small but growing population of super-Earths with measured masses and radii.

2. OBSERVATIONS

We observed 55 Cnc with *MOST* (Microvariability & Oscillations of STars), a Canadian microsatellite equipped with a 15 cm telescope and CCD photometer, capable of short-cadence, long-duration ultraprecise optical photometry of bright stars (Walker et al. 2003, Matthews et al. 2004). *MOST* is in a Sun-synchronous polar orbit 820 km above the terminator with an orbital period of 101 min. Its custom broadband filter covers the visible spectrum (350–700 nm).

We used the Direct Imaging mode, similar to conventional ground-based CCD photometry. The observations spanned a nearly continuous 14.5-day interval from 2011 February 07–22, with four interruptions when fine pointing was lost due to satellite subsystem crashes. Individual exposures lasted 0.5 s but were downloaded in “stacks” of either 40 or 80. The median time sampling in the resulting time series is 43 s, outside of the interruptions.

Data reduction was performed with the method of Rowe et al. (2006), which combines classical aperture photometry and point-spread function fitting to the Direct Imaging subraster of the Science CCD. There are familiar periodic artifacts in the

* Based on data from the *MOST* satellite, a Canadian Space Agency mission, jointly operated by Dynacon Inc., the University of Toronto Institute for Aerospace Studies, and the University of British Columbia, with the assistance of the University of Vienna.

¹ Department of Physics, and Kavli Institute for Astrophysics and Space Research, Massachusetts Institute of Technology, Cambridge, MA 02139

² Department of Physics and Astronomy, University of British Columbia, 6224 Agricultural Road, Vancouver, BC V6T 1Z1, Canada

³ Harvard-Smithsonian Center for Astrophysics, 60 Garden St., Cambridge, MA 02138

⁴ Hubble Fellow

⁵ UCO/Lick Observatory, University of California, Santa Cruz, CA 95064

⁶ University of Vienna, Institute for Astronomy, Türkenschanzstrasse 17, A-1180 Vienna, Austria

⁷ Department of Astronomy and Physics, Saint Mary’s University, Halifax, NS B3H 3C3, Canada

⁸ Département de Physique, Université de Montréal, C.P. 6128, Succ. Centre-Ville, Montréal, QC H3C 3J7, Canada

⁹ NASA Ames Research Center, Moffett Field, CA 94035

¹⁰ Department of Astronomy & Astrophysics, University of Toronto, 50 St. George Street, Toronto, ON M5S 3H4, Canada

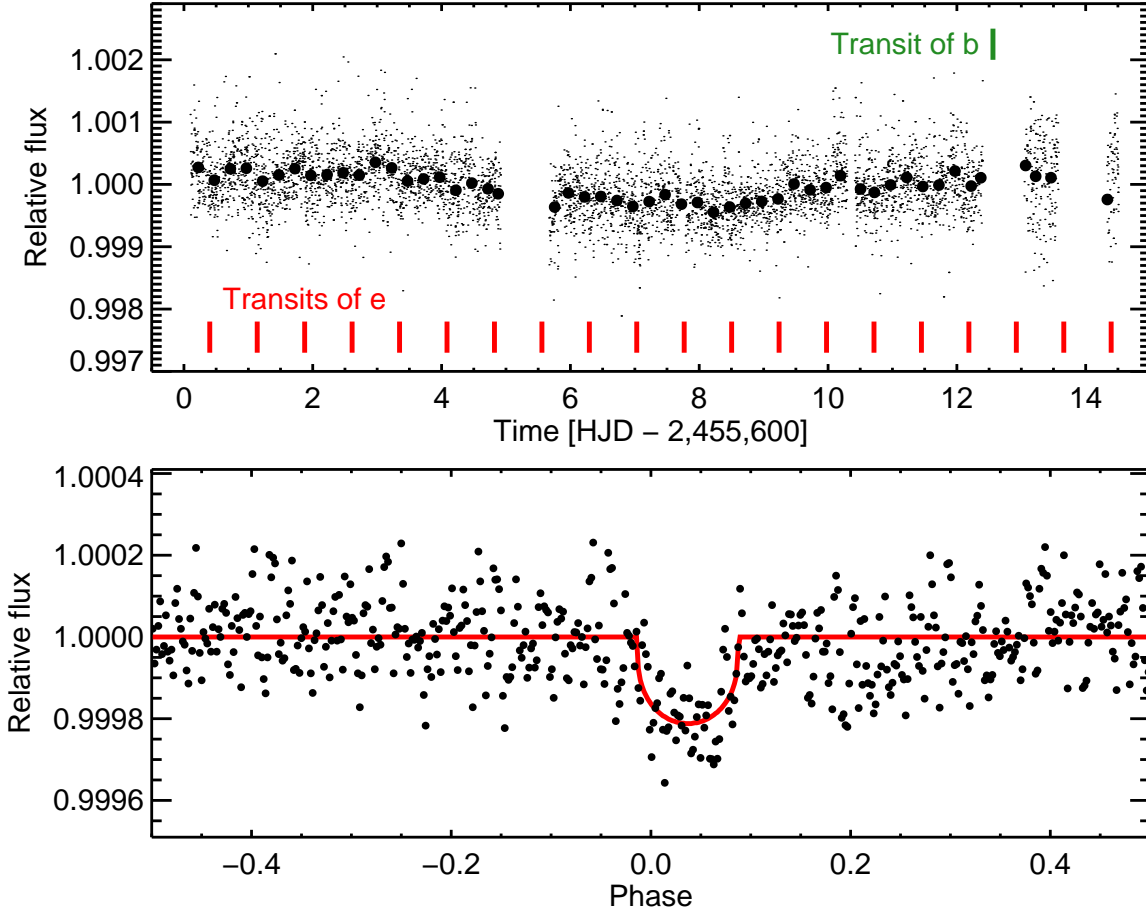


FIG. 1.— *MOST* photometry of 55 Cnc. *Upper*.—The time series. To reduce the file size, a random subset of 10% of the data points are plotted. Large symbols represent 0.25 d averages. Vertical bars mark the 20 predicted transit times of planet e, and the single predicted transit of planet b (which was missed when *MOST* temporarily lost fine pointing). *Lower*.—Phased light curve (after removing the 0.079 d^{-1} trend), folded with $P = 0.736540 \text{ d}$ and $T_c [\text{HJD}] = 2,453,094.6924$ (Dawson & Fabrycky 2010) and averaged into 2 min phase bins (44 data points per bin). The solid curve is the best-fitting transit model.

time series due to scattered Earthshine, appearing at the orbital frequency of the satellite (14.26 d^{-1}) and its lower harmonics, as well as sidelobes arising from the amplitude modulation of the stray light by the Earth’s rotation. Before the transit analysis described below, the artifacts were removed by “prewhitening”: subtracting the best-fitting sinusoids corresponding to the strongest satellite harmonics and sidelobes. This produces minimal effects on the transit signal because the satellite frequency is an order of magnitude higher than the planet orbital frequency. Indeed the transits were detectable even before prewhitening, despite the increased scatter in the phased light curve.

The prewhitened time series is plotted in the upper panel of Figure 1. Variation by a few parts in 10^{-4} is seen on the relatively long timescale of $\sim 10 \text{ d}$, which could be a manifestation of stellar activity and rotation. Fischer et al. (2008) measured a rotation period of $42.7 \pm 2.5 \text{ d}$, which we cannot address given the 14.5 d span of our data. For the transit analysis, the slow variation was filtered out by removing a sinusoid with period 12.6 d.

The lower panel of Figure 1 shows the data after folding with the Dawson & Fabrycky (2010) ephemeris. A significant dip is observed at nearly zero phase, where the transit signal would be expected. We emphasize that the signal shown in Figure 1 is *not* the outcome of a period search. The

data were phased with the *predicted* ephemeris, with no free parameters. Nevertheless, when a period search is performed, the strongest signal is at 0.74 d and there is no signal at the alternative period of 2.82 d . This is demonstrated in Figure 2, which shows a Box-fitting Least Squares periodogram (Kovács et al. 2002). Another measure of the statistical significance of the detection is given in Section 3.

The signal has the predicted period, and the observed epoch is bracketed by the two predicted epochs of Dawson & Fabrycky (2010): it is 35 min later than the circular-orbit prediction and 67 min earlier than the eccentric-orbit prediction. Furthermore the depth and duration of the signal conform with predictions (see Section 3). With close matches to four predicted parameters (period, phase, depth and duration) we consider the existence of transits to be established.

3. ANALYSIS

A transit model was fitted to the light curve based on the formulas of Mandel & Agol (2002) and the Monte Carlo Markov Chain (MCMC) code of Holman et al. (2006) and Winn et al. (2007). The limb-darkening law was taken to be quadratic with coefficients $u_1 = 0.657$ and $u_2 = 0.115$, based on a Kurucz model for a star with $T_{\text{eff}} = 5327 \text{ K}$ and $\log g = 4.48$ (Takeda et al. 2007), integrated over the *MOST* bandpass. The adjustable parameters were the planet-to-star radius ratio

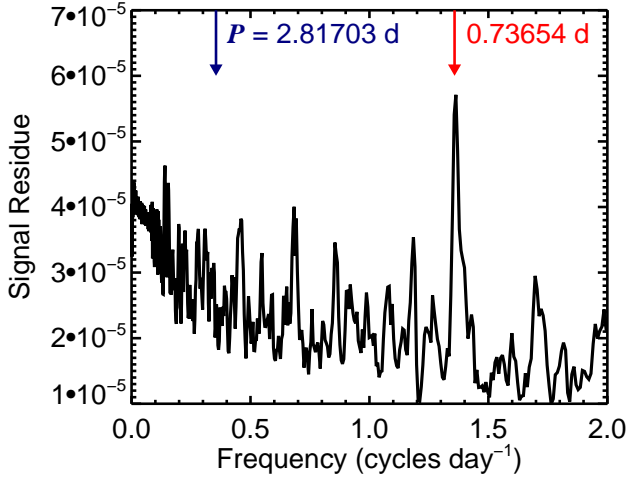


FIG. 2.— **Box-fitting Least Squares frequency spectrum of the MOST data.** Positive peaks indicate detections of candidate transit signals with durations consistent with a near-equatorial transit of 55 Cnc. The strongest peak is at the 0.74 d period, and there is no signal at the 2.81 d period.

R_p/R_* , the star-to-orbit radius ratio R_*/a , the orbital inclination i , and the time of midtransit T_c . The orbit was assumed to be circular. Uniform priors were adopted for R_p/R_* , $\cos i$ and T_c . Because ingress and egress are not well defined in the data, we used Gaussian priors on the stellar radius and mass, $R_* = 1.10 \pm 0.10 R_\odot$ and $M_* = 0.96 \pm 0.10 M_\odot$. The radius prior is based on the interferometrically measured stellar radius (van Belle & von Braun 2009). The mass prior is based on the analysis of the stellar spectroscopic properties by Takeda et al. (2007).¹²

The likelihood was taken to be $\exp(-\chi^2/2)$ with the usual sum-of-squares definition of χ^2 . The 1σ uncertainty in each data point was taken to be the root-mean-square (rms) out-of-transit flux multiplied by a factor β intended to take into account the time-correlated noise. The factor β is the ratio between the standard deviation of residuals binned to 15 min, and the standard deviation one would expect based on the unbinned data assuming white noise (see, e.g., Pont et al. 2006, Carter & Winn 2009). The rms and β values were 90 ppm and 1.31, respectively.

There are 530 data points in the binned light curve, and the model has essentially 3 free parameters (depth, duration, and central phase), giving 527 degrees of freedom. The reduction in χ^2 by fitting a transit model, as compared to a straight line, is $\Delta\chi^2 = 146$, representing a highly significant detection. Table 1 gives the results for the model parameters, based on the marginalized posteriors of the Markov chains.

4. DISCUSSION

4.1. Comparison to theoretical models

Both the mass and radius of 55 Cnc e are known to within 10%, providing a valuable example with which to test theoretical models of super-Earth structure. To provide a broad view, the left panel of Figure 3 shows the masses and radii of the transiting exoplanets for which both quantities have

been measured, along with theoretical curves taken from Seager et al. (2007) for “mathematicians’ planets” composed of pure hydrogen, water, rock (MgSiO_3 perovskite) and iron. 55 Cnc e falls between the rock and iron lines, suggesting a rock-iron composition similar to Earth. The right panel of Figure 3 shows some theoretical curves based on more detailed models. In the models of Valencia et al. (2006), for example, a planet of this mass should have a radius of 1.7 – $1.8 R_\oplus$, within the uncertainty of the measured radius.

4.2. Possibility of an atmosphere

We estimated the maximum possible mass of an atmosphere in a manner similar to the approach taken by Charbonneau et al. (2009). We assumed the solid portion of the planet has a radius of $1.4 R_\oplus$, which Marcus et al. (2010) argued is the smallest plausible radius for a planet of this mass, obtained in the limit of maximum stripping of the mantle by giant impacts. We added an isothermal atmosphere composed of 75% hydrogen and 25% helium with a pressure of 1 mbar at a height of $1.8 R_\oplus$ (the 1σ upper bound on the measured radius). The outcome of this calculation was that any atmosphere likely comprises less than 0.01% of the planet’s mass.

Any atmosphere around 55 Cnc e would be strongly heated, as the planet is located only $3 R_*$ from the host star. The temperature at the substellar point could be as high as 2970 K if the planet is tidally locked and the incoming heat remains on the dayside. If the heat is redistributed evenly over the planet’s entire surface, the equilibrium temperature could be 2100 K, assuming an albedo of zero.

It is questionable whether an atmosphere could be retained in such infernal conditions. We estimated the energy-limited hydrodynamic escape rate using Eqn. (19) of Murray-Clay et al. (2009). To estimate the UV flux we used Eqn. (1) of Ribas et al. (2005) for an assumed age of 5 Gyr, giving $1.6 \times 10^4 \text{ erg s}^{-1} \text{ cm}^{-2}$. Then, assuming 30% of the incident power of the ionizing radiation is available to do work on the atmosphere, the escape rate is $\sim 5 \times 10^9 \text{ g s}^{-1}$ and the total mass loss over 5 Gyr is $\sim 0.02 M_p$, several orders of magnitude larger than maximum atmospheric mass. Thus it seems unlikely that 55 Cnc e retains any primordial low-molecular-weight atmosphere, although it is possible that tectonic activity replenishes a thin high-molecular-weight atmosphere. No firm conclusions are possible due to the large uncertainties involved, but one observational test would be to measure the thermal phase curve and the location of the hottest portion of the planet. An atmospheric wind could act to shift the hot spot away from the substellar point (see, e.g., Knutson et al. 2007).

4.3. Comparison with other super-Earths

55 Cnc e is one of a growing number of super-Earths with measured masses and radii, allowing us to compare their physical properties and gain clues about their formation and evolution. The right panel of Figure 3 focuses on the super-Earths and indicates the contours of constant mean density. The trio of Kepler-10b (Batalha et al. 2011), CoRoT-7b (Léger et al. 2009) and 55 Cnc e all have high densities, while GJ 1214b (Charbonneau et al. 2009) and Kepler-11d, e, and f (Lissauer et al. 2011) have much lower densities. A striking contrast exists between 55 Cnc e and Kepler-11e, which have similar masses but densities differing by a factor of 20.

It may be relevant that the higher-density super-Earths are subject to more intense insolation. They all orbit G stars with periods < 1 day. In contrast, the lower-density Kepler-11 planets have periods 10–50 days, and GJ 1214b orbits a much

¹² Takeda et al. (2007) advocate a smaller uncertainty, $M_* = 0.963^{+0.051}_{-0.029} M_\odot$, but the same analysis led to $R_* = 0.930^{+0.040}_{-0.030} M_\odot$ which disagrees by 1.6σ with the interferometrically measured radius. Therefore we enlarged the mass uncertainty to $0.10 M_\odot$.

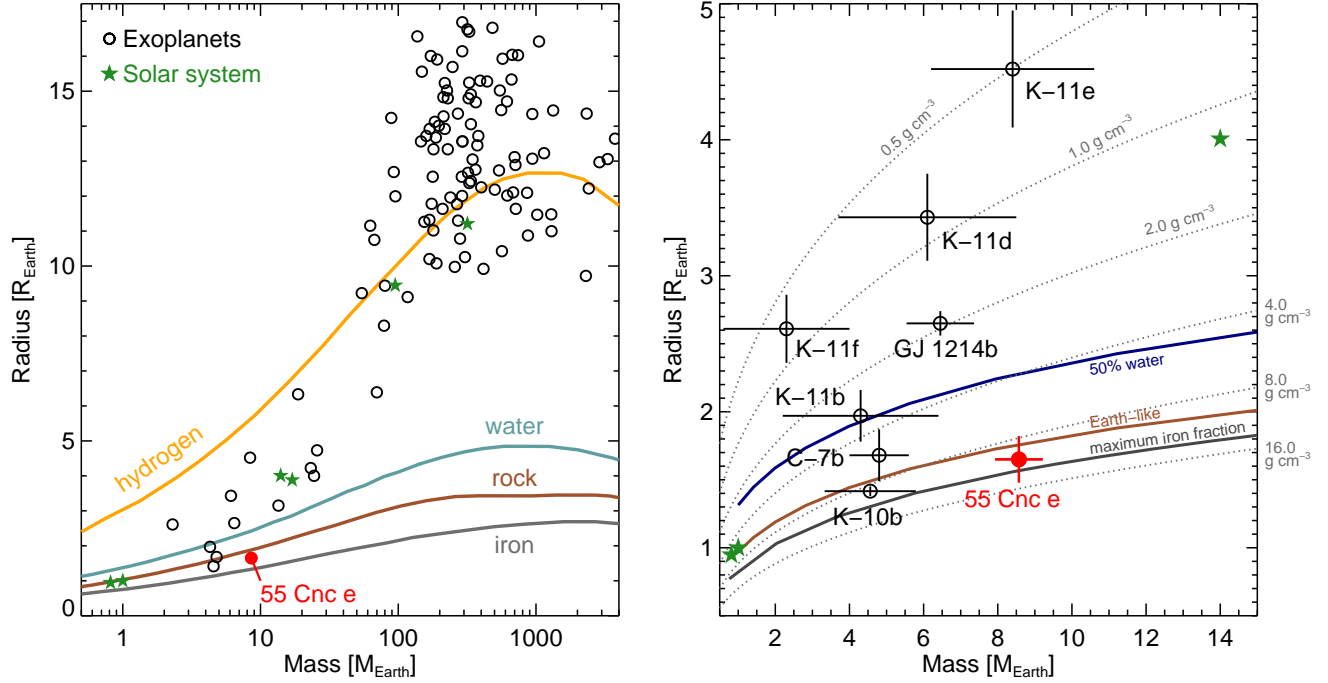


FIG. 3.— **Masses and radii of transiting exoplanets.** Open circles (blue) are previously known transiting planets. The filled circle (red) is 55 Cnc e. The stars (green) are Solar system planets, for comparison. *Left.*—Broad view, with curves showing mass-radius relations for pure hydrogen, water ice, silicate (MgSiO_3 perovskite) and iron, from Figure 4 of Seager et al. (2007). *Right.*—Focus on super-Earths, showing contours of constant mean density and a few illustrative theoretical models: a “water-world” composition with 50% water, 44% silicate mantle and 6% iron core; a nominal “Earth-like” composition with terrestrial iron/silicon ratio and no volatiles (Valencia et al. 2006, Li & Sasselov, submitted); and the maximum mantle stripping limit (maximum iron fraction, minimum radius) computed by Marcus et al. (2010).

cooler M dwarf. Perhaps we are witnessing the consequences of atmospheric escape and mass loss due to strong stellar irradiation. This interpretation is not unique, though, because there are other possible routes to producing high-density planets, such as giant impacts (Marcus et al. 2010).

4.4. Orbital coplanarity

55 Cnc e is the innermost planet in a system of at least five planets. If the orbits are coplanar and sufficiently close to 90° inclination, then multiple planets would transit. Transits of b and c were ruled out by Fischer et al. (2008).¹³ However, those nondetections do not lead to constraints on mutual inclinations. Given the measured inclination for planet e of $90^\circ \pm 9^\circ$, the other planets in the system could be perfectly aligned with planet e and still fail to transit.

McArthur et al. (2004) reported an orbital inclination $53^\circ \pm 6.8^\circ$ for the outermost planet d, based on a preliminary investigation of *Hubble Space Telescope* astrometry. This would imply a strong misalignment between the orbits of d and e. However, the authors noted that the astrometric dataset spanned only a limited arc of the planet’s orbit, and no final results have yet been announced. Additional astrometric measurements and analysis are warranted before delving into the interpretation of any orbital misalignment.

¹³ Our *MOST* observation might have led to even firmer results for planet b, since it spanned a full orbit of that planet, but unfortunately no useful data were obtained during the transit window because of a satellite subsystem crash (see Fig. 1). The *MOST* observation did not coincide with any transit windows for planets c-f.

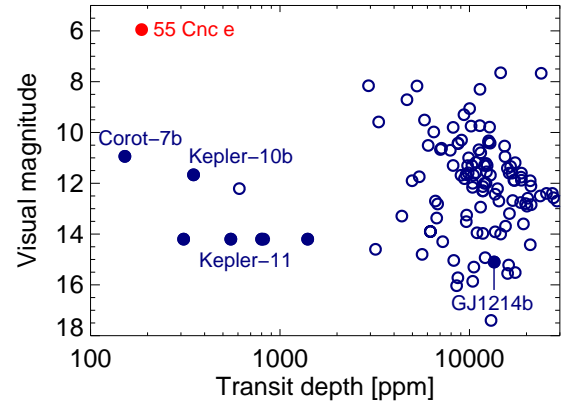


FIG. 4.— **Stellar brightness and transit depths.** The V band magnitudes and transit depths $(R_p/R_\star)^2$ of the transiting planets with known masses and radii. Solid symbols are super-Earths ($M_p \gtrsim 10 M_\oplus$).

4.5. Potential for follow-up observations

Figure 4 shows an observer’s view of the transiting planets. Plotted are two parameters directly related to the feasibility of follow-up observations: stellar brightness and transit depth. 55 Cnc e has a uniquely bright host star, towering above the other super-Earth hosts and nearly 2 mag brighter than any other transit host. Even in the near-infrared, where GJ 1214 emits a larger fraction of its luminosity, 55 Cnc is about 5 mag brighter. However, Figure 4 also shows that the transit depth for 55 Cnc e is among the smallest known. This combination

of factors causes the follow-up landscape for 55 Cnc e to differ from that of other planets.

The shallow depth makes certain follow-up observations challenging despite the abundance of photons. To resolve the transit ingress and egress, and thereby improve estimates of the planet's orbital inclination and absolute dimensions, it will be necessary to improve the signal-to-noise ratio in the phased light curve. This will require observations of more transits, or the use of larger-aperture telescopes. More daunting, but within the realm of possibility, is the detection of occultations and orbital phase variations that might betray the presence of an atmosphere. The order of magnitude of those effects is governed by the parameter $(R_p/a)^2 \sim 2 \times 10^{-5}$.

Transit timing constraints on the system's architecture will not be easily obtained, given the shallow transit as well as the small amplitudes of the expected signals. Even planet b, the nearest planet to e, is expected to perturb e's transit epoch by less than 1 s over the course of its 14 d period. The most readily detectable effect may be the Römer delay due to planet d, which should cause a sinusoidal variation in planet e's transit epoch with peak-to-trough amplitude of 12 s and period 5191 d.

On the other hand, follow-up observations of the star itself are far easier than for other transit hosts, and will continue to be rewarding. Already the stellar radius has been measured interferometrically (van Belle & von Braun 2009), the optical spectrum has revealed chemical peculiarities (as summarized

by Takeda et al. 2007), the stellar variability has been tracked for 11 years (Fischer et al. 2008), and there is potential for future observations such as the detection of *p*-mode oscillations that would help define the stellar properties (see, e.g., Gilliland et al. 2011, Nutzman et al. 2011). Furthermore, the brightness of the star has already facilitated the discovery of other planets in this system, and continued monitoring has a greater potential to reveal additional bodies than is the case for fainter stars.

Finally, there is some pleasure in being able to point to a naked-eye star and know the mass and radius of one of its planets.

We thank Laura McKnight and Andrew Howard for helpful conversations. J.M., D.G., A.M., and S.R. thank NSERC (Canada) for financial support. T.K. is supported by a contract to the Canadian Space Agency. R.K. and W.W. were supported by the Austrian Science Fund. D.D. is supported by a FQRNT scholarship. R.D. is supported by a National Science Foundation Graduate Research Fellowship, and D.C.F. by a NASA Hubble Fellowship through grant HF-51272.01-A. M.H. and J.W. gratefully acknowledge support from the NASA Origins program through award NNX09AB33G.

REFERENCES

- Batalha, N. M., et al. 2011, *ApJ*, 729, 27
 Butler, R. P., Marcy, G. W., Williams, E., Hauser, H., & Shirts, P. 1997, *ApJ*, 474, L115
 Carter, J. A., & Winn, J. N. 2009, *ApJ*, 704, 51
 Charbonneau, D., et al. 2009, *Nature*, 462, 891
 Dawson, R. I., & Fabrycky, D. C. 2010, *ApJ*, 722, 937
 Fischer, D. A., et al. 2008, *ApJ*, 675, 790
 Gilliland, R. L., McCullough, P. R., Nelan, E. P., Brown, T. M., Charbonneau, D., Nutzman, P., Christensen-Dalsgaard, J., & Kjeldsen, H. 2011, *ApJ*, 726, 2
 Holman, M. J., et al. 2006, *ApJ*, 652, 1715
 Ji, J., Kinoshita, H., Liu, L., & Li, G. 2003, *ApJ*, 585, L139
 Knutson, H. A., et al. 2007, *Nature*, 447, 183
 Kovács, G., Zucker, S., & Mazeh, T. 2002, *A&A*, 391, 369
 Léger, A., et al. 2009, *A&A*, 506, 287
 Lissauer, J. J., et al. 2011, *Nature*, 470, 53
 Lovis, C., et al. 2011, *A&A*, 528, A112
 Mandel, K., & Agol, E. 2002, *ApJ*, 580, L171
 Marcus, R. A., Sasselov, D., Hernquist, L., & Stewart, S. T. 2010, *ApJ*, 712, L73
 Marcy, G. W., Butler, R. P., Fischer, D. A., Laughlin, G., Vogt, S. S., Henry, G. W., & Pourbaix, D. 2002, *ApJ*, 581, 1375
 Matthews, J. M., Kuchner, R., Guenther, D. B., Walker, G. A. H., Moffat, A. F. J., Rucinski, S. M., Sasselov, D., & Weiss, W. W. 2004, *Nature*, 430, 51
 McArthur, B. E., et al. 2004, *ApJ*, 614, L81
 Mugrauer, M., Neuhauser, R., Mazeh, T., Guenther, E., Fernández, M., & Broeg, C. 2006, *Astronomische Nachrichten*, 327, 321
 Murray-Clay, R. A., Chiang, E. I., & Murray, N. 2009, *ApJ*, 693, 23
 Nutzman, P., et al. 2011, *ApJ*, 726, 3
 Pont, F., Zucker, S., & Queloz, D. 2006, *MNRAS*, 373, 231
 Ribas, I., Guinan, E. F., Güdel, M., & Audard, M. 2005, *ApJ*, 622, 680
 Rowe, J. F., et al. 2006, *ApJ*, 646, 1241
 Seager, S., Kuchner, M., Hier-Majumder, C. A., & Militzer, B. 2007, *ApJ*, 669, 1279
 Takeda, G., Ford, E. B., Sills, A., Rasio, F. A., Fischer, D. A., & Valenti, J. A. 2007, *ApJS*, 168, 297
 Valencia, D., O'Connell, R. J., & Sasselov, D. 2006, *Icarus*, 181, 545
 van Belle, G. T., & von Braun, K. 2009, *ApJ*, 694, 1085
 Walker, G., et al. 2003, *PASP*, 115, 1023
 Winn, J. N., Holman, M. J., & Roussanova, A. 2007, *ApJ*, 657, 1098
 Winn, J. N. 2010, in *Exoplanets*, ed. S. Seager (Tucson: University of Arizona Press)
 Wisdom, J. 2005, *Bulletin of the American Astronomical Society*, 37, 525

TABLE 1
SYSTEM PARAMETERS FOR 55 CNC E

Parameter	Value
Orbital period, P [d]	0.736540 ± 0.000003
Midtransit time [HJD]	$2,455,607.0553 \pm 0.0026$
Planet-to-star radius ratio, R_p/R_*	0.01356 ± 0.00078
Transit duration, first to fourth contact [d]	0.0734 ± 0.0054
Transit ingress or egress duration [d]	$0.00116^{+0.00031}_{-0.00014}$
Transit impact parameter	0.00 ± 0.45
Orbital inclination, i [deg]	90.0 ± 8.6
Fractional stellar radius, R_*/a	0.3278 ± 0.026
Fractional planetary radius, R_p/a	$0.00441^{+0.00053}_{-0.00037}$
Orbital distance, a [AU]	0.01573 ± 0.00054
Planetary mass [M_\oplus]	8.57 ± 0.64
Planetary radius [R_\oplus]	1.63 ± 0.16
Planetary mean density [g cm^{-3}]	10.9 ± 3.1
Planetary surface gravity [m s^{-2}]	31.7 ± 6.1

NOTE. — These parameters were determined by fitting the *MOST* light curve as described in the text, in combination with external constraints on the stellar reflex velocity $K_* = 6.1 \pm 0.2 \text{ m s}^{-1}$, stellar mass $M_* = 0.96 \pm 0.10 M_\odot$ (Takeda et al. 2007, with an enlarged uncertainty), and stellar radius $R_* = 1.10 \pm 0.10 R_\odot$ (van Belle & von Braun 2009). We further assumed the orbital eccentricity to be zero, and the limb-darkening law to be quadratic with fixed coefficients $u_1 = 0.657$ and $u_2 = 0.115$.